ISBN: 978-3-95450-221-9 ISSN: 2226-0358 doi:10.18429/JACoW-ICALEPCS2021-WEPV001

TEMPERATURE CONTROL FOR BEAMLINE PRECISION SYSTEMS OF SIRIUS/LNLS

J.L.N. Brito*, G. S. Baldon, F. R. Lena, M. A. L. Moraes, R. R. Geraldes, M. Saveri Silva, L. M. Volpe, Brazilian Synchrotron Light Laboratory (LNLS), CNPEM, Campinas, Brazil

Abstract

Precision beamline systems, such as monochromators and mirrors, as well as sample stages and sample holders, may require fine thermal management to meet performance targets. Regarding the optical elements, the main aspects of interest include substrate integrity, in case of high power loads and densities; wavefront preservation, due to thermal distortions of the optical surfaces; and beam stability, related to thermal drift. Concerning the sample, nanometer positioning control, for example, may be affected by thermal drifts and the power management of some electrical elements. This work presents the temperature control architecture developed in house for precision elements at the first beamlines of Sirius, the 4th-generation light source at the Brazilian Synchrotron Light Laboratory (LNLS). Taking some optical components as case studies, the predictive thermal-model-based approach, the system identification techniques, the controller design workflow and the implementation in hardware are described, as well as the temperature stability results.

INTRODUCTION

To address strict performance challenges of the new-generation beamlines at the Sirius 4th-generation light source [1], a series of innovative instruments have been developed in-house by the the Brazilian Synchrotron Light Laboratory (LNLS) over the past few years. Considered critical elements, special attention was given to optical systems – such as the High-Dynamic Double-Crystal Monochromator (HD-DCM) [2], the 4-bounce Crystal Monochromator (4CM) [3], mirror systems [4] and experimental stations [5].

These high-performance systems have been developed according to strong precision engineering and mechatronics principles, in which mechanical, thermal, metrology, control, and software aspects must be jointly addressed since early design stage [6]. Within this scope, sub-system functionalities are decoupled as much as possible from each other to minimized crossed effects, such that, as an example, a cooling system aims to be mechanically decoupled from the element of interest, whereas a positioning system/structure tends to be thermally decoupled from it.

Oftentimes, flexural structures are used as predictive solutions for kinematic mounts and fine positioning capabilities, with complementary thermal isolation possibilities [4, 7, 8]. Indeed, thermal decoupling is an essential aspect in many of these systems because cryogenic solutions were extensively adopted, either for sample conditioning [8], or for the silicon-based optical elements [2–4], to benefit from the thermal properties of this material at low temperatures in handling heat dissipation and thermal stresses/deformations.

Next, in addition to thermal decoupling, temperature control becomes an indispensable feature in many of these systems, being used for: 1) coarse static compensation in heat-flow for the desired operation temperatures; 2) heat load compensation (with and without beam, for example); 3) reduction of the time constants in the closed-loop systems as compared to passive or open-loop response; and 4) fine temperature control in drift-sensitive systems.

The following sections present the temperature control architecture that has been standardized for some Sirius beamline systems; the hardware, with appropriate actuators and sensors being critical for robust and high-performance control capabilities; predictive and experimentally derived plant models; and illustrative commissioning examples.

ARCHITECTURE AND HARDWARE

The hardware architecture adopted to control the temperature of the Sirius precision beamline systems is summarized in the Fig. 1, where a NI CompactRIO (cRIO) implements the control by reading the temperature sensors and acting through heaters present in the system, represented by a mirror. The cRIO also interfaces with the equipment protection system (EPS) [9], closing the beam shutter in case of overheating or disabling the cooling system to prevent overcooling, for example.

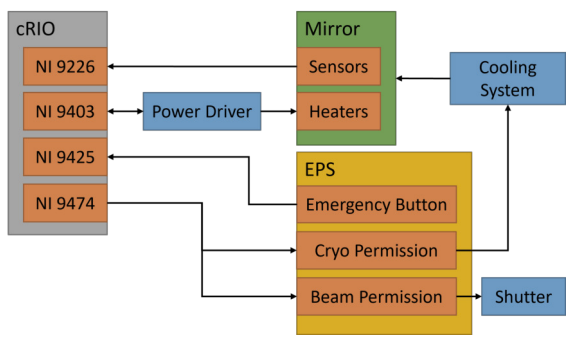

Figure 1: Temperature control hardware architecture.

The elements of the architecture and its characteristics are presented below.

Power Driver

The power driver is a multi-channel heater driver [10] in-house developed with 8 channels that delivers up to 1.5 A at 12 V DC per channel, where the voltage output

* joao.brito@lnls.br

ISBN: 978-3-95450-221-9 ISSN: 2226-0358 doi:10.18429/JACoW-ICALEPCS2021-WEPV001

is controlled via a 5 V PWM input signal. Each channel has also a 5 V TTL input to power enable and a 5 V TTL failure output to indicate that the power was tuned off due to an open-load or short-circuit.

cRIO

The cRIO platform has been adopted in solutions involving data acquisition, synchronization [11], temperature and high-dynamic motion control [12] for the beamlines, as a rugged platform that combines the high-speed logic and determinism of an FPGA with the flexibility of a real-time processor. The currently used cRIO chassis, i.e. cRIO-9039, cRIO-9045, cRIO-9048 and cRIO-9049, have 8 slots to which a variety of digital and analog I/O modules can be plugged in, allowing one or more solutions to be implemented on the same chassis.

In the temperature control setup, the EPS interface is done by one NI 9425, a 32-channel digital input module compatible with 24V logic level, and one NI 9474, a digital output module compatible with 5 V to 30 V. The chosen module for reading the temperature sensors was the NI 9226, an 8-channel RTD (Resistance Temperature Detector) analog input with 24 bits of resolution, 0 to 4 kΩ measurement range and a 3 and 4-wire connection compatibility. To drive the heaters, each channel in the power driver needs to receive two signals, namely, PWM and power enable, and returns a failure one. For this task the NI 9403 was selected, which is a 32- channel, 5 V TTL bidirectional digital I/O module.

EPS

The EPS is a safety application implemented in a programmable logic controller (PLC) that monitors diverse beamline systems to protect the instruments against incidents as vacuum loss, high temperature, power outage and more, as well as manages the interlock beamline system.

Cooling Systems

The general temperature control hardware architecture of most of the beamline instrumentation is based on a cryogenic heat sink, controlled thermal masses, and electric heaters as thermal actuators with sensing nodes determined by temperature sensors. For liquid nitrogen (LN_2) cooling systems like monochromators and cryogenic mirrors, that use closed-loop cryocoolers and open-cycle cryostats, respectively, the minimum heat sink temperature is determined by the vaporization temperature of the cooling liquid, being approximately 77 K at the current pressure configurations.

More recently, helium (He) pulse tubes started to be considered for forthcoming ultra-high vacuum (UHV) applications as well. As compared to the (LN_2) cryostats and cryocoolers, the He pulse tube prevents the consumption of the coolant, which is a significant operational advantage. Moreover, the cost of a typical beamline cryocooler is much higher than that of a typical cryostast or pulse-tube, which justifies its use only in very specific cases. In addition, the pulse tube should minimize operational issues that have been found in the cryostats, such as sensitivity to the phase transitions (icing, clogging and vibrations) and temperature oscillations in the load due to variations in the Dewar pressure. Indeed, in the pulse tube the flow is controlled by the frequency of the compressor, where are located the moving parts, that can be mechanically decoupled from the cold tip. Limitations in the pulse tube are essentially related to their load capacities, which are not sufficient for many beamline application.

UHV Heaters

The first cryogenic systems at Sirius beamlines utilized two different thin-film, UHV-compatible Kapton heaters from Taiwan KLC (part number TSC013D003GR36Z01), with nominal resistances of 36 Ω and 14.4 Ω for 4 W and 10 W power at 12 V, respectively. Although having an easy integration and proven vacuum compatibility, along with low cost, the flexible nature of the Kapton heaters made the clamping to the components a potential source of failure. Indeed, the components surface characteristics, together with human errors during the assembly process, often led to crushing of the electric track, or to bad contact interface, thus resulting in open or short circuits, overheating and failure. Also, it was found that these heaters might contaminate the vacuum systems in a failure event, due to outgassing. All these aspects reduce the systems robustness, increasing the need of corrective maintenance and posing risks to the sensitive optics.

Therefore, a new heating element is under development for higher reliability. As depicted in Fig. 2, it consists of an SMD (Surface Mount Device) nickel thin film and alumina power resistor from Susumu, soldered over a small aluminium metalcore PCB (Printed Circuit Board) using a lead free (SAC305) solder paste. The board is then encapsulated inside a small aluminium case using the Stycast 2850FT epoxy resin along with CAT11 catalyser. The aluminum PCB and housing serve as efficient heat condutors to the part of interest.

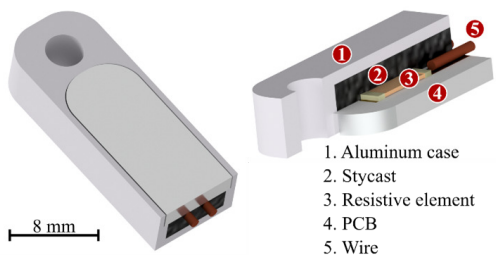

Figure 2: Heater 3D model and internal elements.

Heaters for 4.4 W and 8 W nominal power at 12 V were extensively tested for lifetime and outgassing by cycling them between 60 K and 390 K, as shown in Fig. 3. After 250 cycles, 3 of the 12 heaters tested failed, always within the first 20 cycles, which was observed by the heaters appearing as an open circuits for the power driver. For reference, initial tests with 7 heaters soldered with 63-37% tin-lead alloy did not present failures during all 82 tested cycles between 80 K

ISBN: 978-3-95450-221-9 ISSN: 2226-0358 doi:10.18429/JACoW-ICALEPCS2021-WEPV001

to 390 K, indicating that the lead-free solder could be the major culprit.

In fact, the lead-free soldering temperature is higher (220 °C versus 183 °C), making it harder to manually solder by hot air. Then, two possible solutions to the solder problem are: hiring the services of a specialized company for the soldering, allowing for a more consistent process; or ditching the lead-free solder altogether, since the tin-lead solder did not present those problems, which might offer residula risks in terms of vacuum compliance. One last aspect to consider is that, during the whole cycling test, no excessive outgassing was observed (see Fig. 3), which was an important step for validating this heater for UHV systems. Future monochromators, mirror systems and vacuum sample environments will be using the new heaters.

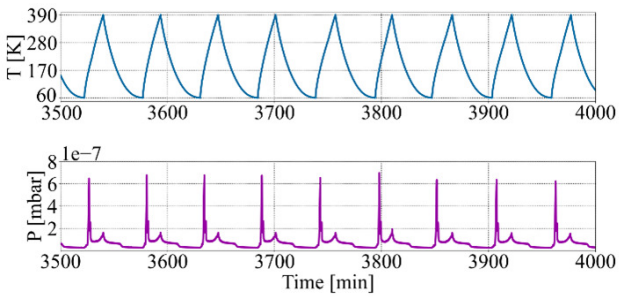

Figure 3: Fatigue and outgassing validation tests for the new heaters: cycling temperatures (top) and pressure (bottom).

Temperature Sensors

The temperature sensors also had design iteration since the beginning of the commissioning of the first cryogenic beamline instrumentation.Initially, 10k Ohm (0°C nominal) Platinum thin-film RTD sensors from IST (P10K.520.6W.B.010.D) were used for parts in operating temperature below 123 K, whereas ceramic Amphenol DC95F202WN negative temperature coefficient (NTC) sensors were used above 270 K, usually at room temperature components equal to 297 K. The part-though-hole (PTH) sensors were soldered to thin, 30 AWG, varnish insulated copper wires with small amounts of tin-lead (70/30) alloy. The set was then encapsulated with the same Stycast resin into small aluminium cases for thermal conductivity and mounting features.

The strategy with different sensors for different temperature intervals was chosen to better use the full sensing range of the NI 9226 (see Fig. 1), resulting in a temperature resolution better than 0.1 mK for both sensors at their nominal operational temperatures, as shown in Fig. 4. However, it has been recently concluded that, for most applications, it would be advantageous to trade the higher resolution by the possibility of measuring a broader temperature range, namely, the full range from the LN_2 cryogenic condition up to the optics typical baking temperature (> 85 °C).

Furthermore, the thin platinum wire of the 10 kΩ RTDs presented bad solderability and its assembly process was too laborious, resulting in unreliable mechanical bonds and a failure rate beyond acceptable for a robust beamline instrumentation. The alternative was to use 2 kΩ IST RTDs (P2K0.232.3FW.B.007) with custom-made flat gold-platted terminals, resulting in a full range sensor with better solderability and temperature resolution below 0.4 mK over the entire measurable range (see Fig. 4).

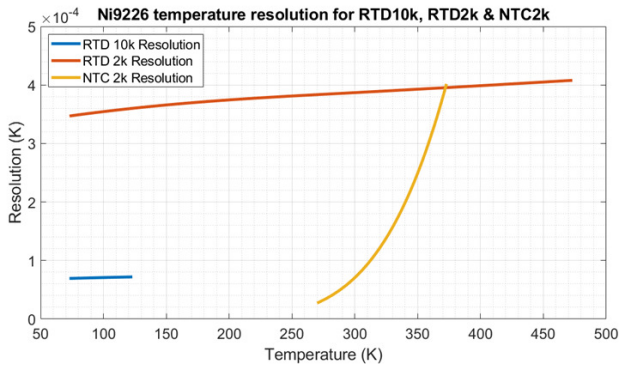

Figure 4: Temperature resolution over the measurable range for the three sensors and NI 9226 at high resolution mode.

The final design of the new sensor in depicted in Fig. 5. The encapsulating process is similar, with just slight geometry changes to simplify assembly. For validation, a few units were cycled for fatigue in the same test setup of the heaters (see Fig. 3), ultimately being totally operational. Dozens of these sensors are currently operational at the beamlines with no failure detected. Finally, as a next step towards improved control accuracy, a sensor calibration setup is currently in development and will be presented in a future work.

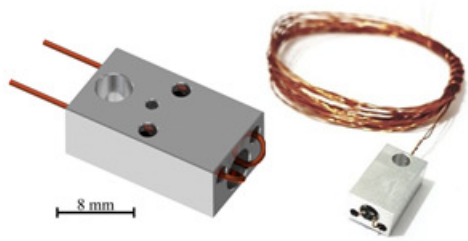

Figure 5: Temperature sensor assembly.

CONTROLLER DESIGN

Assuming that a certain knowledge about the plant to be controlled is necessary to specify the control architecture and its parameters, the controller design workflow described below initiates with predictive thermal modeling combined with a system identification method. After that, a model to estimate the plant behavior is defined and a proposed controller is simulated, implemented and validated with the real plant.

ISBN: 978-3-95450-221-9 ISSN: 2226-0358 doi:10.18429/JACoW-ICALEPCS2021-WEPV001

Predictive Thermal Modeling

To develop a predictive thermal model for each precision beamline system, lumped mass thermal models have been implemented together with auxiliary finite elements analyses (FEA) to simulate the system behavior under variable operational conditions, taking into account also non-linear aspects [4, 7, 13].

The predictive models have contributed to validate and improve thermal modeling, not only defining power requirements for control heaters and an initial guess to the controller parameters, but also diagnosing system issues, as the manufacturing limitations. Furthermore, during the design phase the lumped-mass models make the system parts sizing faster than by using only FEA. Recently, with experience and customized modeling tools, the differences found between model predictions and measurements have been below 10 K, as presented in [13].

System Identification

As mentioned, a relevant aspect about the beamline precision systems is that, although they are composed of different parts operating at different temperatures, these parts are designed to be thermally decoupled [4]. This has been confirmed during the predictive thermal model validation and also during the system identification process, in which the observed thermal coupling is negligible. Because of this, the systems can be seen as a set of isolated single-input single-output (SISO) plants.

Since the controller's goal is to keep the plant temperature stable, the system identification approach was used to find an approximate linear model of each SISO plant for a given operation condition defined by the desired operating temperature.

Taking the HD-DCM from the EMA beamline as a study case, which is a 14-SISO-plant system with 2 plants operating at −118 °C, 3 at −6 °C and 9 at 18 °C, system identification based on the step response was performed to estimate continuous-time transfer functions (TFs) for the plants, described in the Laplace domain by

$$\frac{Y(s)}{U(s)} = \frac{k}{(s-p)},$$

where s is the Laplace variable, $Y(s)$ is the sensor output in Celsius, $U(s)$ is the power input in W, k is the dc gain and p the pole of the transfer function.

After a set of data acquisitions with the system around the operating temperature for plant identification and TF estimation, another set at slightly different temperatures was selected for validation of the estimated plants. In the latter, the temperatures were taken only a few tens of degrees off, to prevent exceedingly large variations of the non-linear materials thermal properties. Figure 6 shows an example with results of both the identification and the validation sets, obtained for one of the HD-DCM crystals, the most critical element in that system whose desired operating temperature is −118 °C and maximum estimation error found during the validation process was less than 0.7 °C. For the other 14 plants, the estimation error remained below 1 °C.

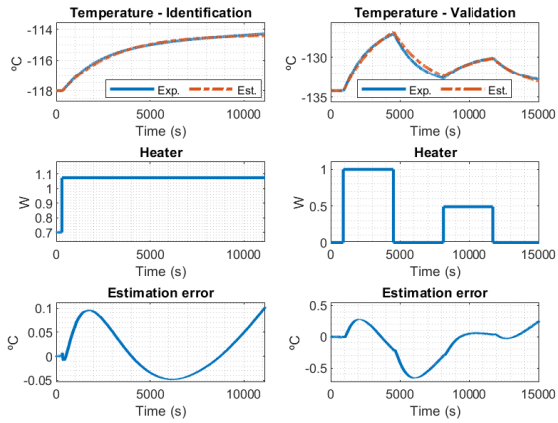

Figure 6: Experimental and identified estimation results of system identification (step response) (left) and validation (right) for the HD-DCM crystal at the EMA beamline.

Controller

Due to its robustness and ease of tuning and implementation, a proportional integral derivative (PID) controller was selected as the first choice to implement the temperature control for the beamline precision systems. As the controller should be implemented in a digital platform, it was designed in the discrete time domain, in which the ideal PID transfer function is represented by

$$PID(z) = \frac{U(z)}{E(z)} = k_p + \frac{k_i.T_s.z}{z-1} + \frac{k_d(z-1)}{T_s.z},$$

where $U(z)$ is the controller output, $E(z)$ is the controller input, defined by the difference between the temperature setpoint and the plant output temperature sensor, k_p is the proportional gain, k_i is the integral gain, k_d is the derivative gain and T_s is the sampling time.

However, the ideal PID has some undesired effects that need to be avoided. Firstly, about the derivative implementation, an instant variation in the temperature setpoint or even the noise produced by the temperature sensor can cause high derivative response, resulting in unreasonable control output. Thus, to prevent this behavior, the following PID with derivative filtering was implemented

$$PIDF(z) = \frac{U(z)}{E(z)} = k_p + \frac{k_i.T_s.z}{z-1} + \frac{k_d}{T_f + \frac{T_s.z}{z-1}},$$

where T_f is the derivative filter time constant.

Then, another undesired effect is the integral windup, caused by the continuous integration of the input $E(z)$ by the integral term even when the power driver output is saturated. Hence, an anti-windup scheme is implemented to turn off the integral term ($k_i = 0$) when the controller output reaches the limits of the power driver.

ISBN: 978-3-95450-221-9 ISSN: 2226-0358 doi:10.18429/JACoW-ICALEPCS2021-WEPV001

Results

Once the plants were identified and the controller model was selected,the controller parameters were calculated to minimize the closed-loops settling time, while keeping the overshoot within less than 10% to a step response. Still considering the HD-DCM crystal from EMA, Fig. 7 shows the experimental and estimated closed-loop step response with a 0.05 °C variation in the setpoint input. In this case, the settling time to within 10% is only 10 min, as compared to the time constant of 1.5 h of the open-loop response, seen in the identification plot in Fig. 6. Similar performances were also achieved in the other controllers.

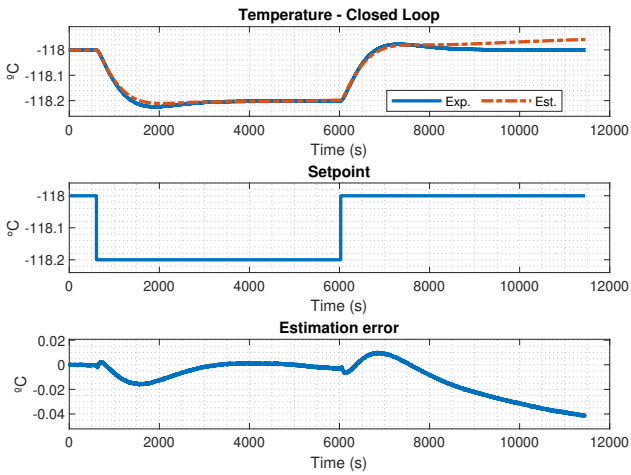

Figure 7: Simulated and experimental closed-loop step response for the HD-DCM crystal at the EMA beamline.

Then, looking at the long-term temperature stability, a variation of less than 0.004 °C is observed in the 12-hour plot presented in Fig. 8, with the larger dip possibly related to a refilling event in the cryocooler.

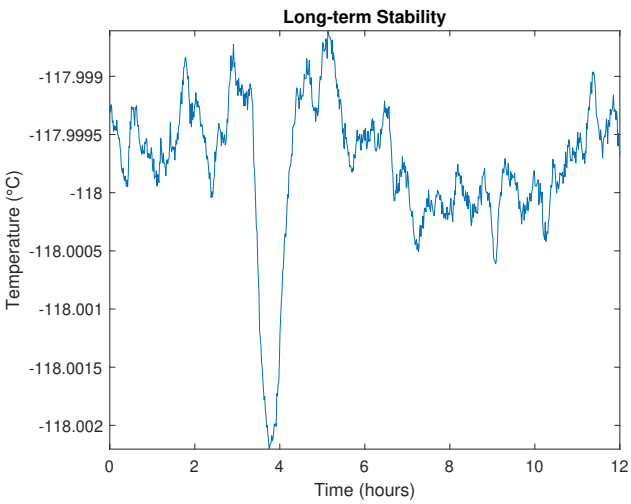

Figure 8: Long-term closed-loop thermal stability in the HD-DCM crystal at the EMA beamline.

CONCLUSION

This work presented the system architecture, the main hardware, and the controller design workflow adopted to the temperature control of Sirius beamline precision systems, where the predictive thermal modeling combined with the system identification approach contributed to define suitable controllers to achieve the design requirements. For reliable and robust beam delivery and experimental conditions, in addition to static compensation at nominal operating temperatures, control levels down to the mK range are, indeed, welcome and desired for ultimate performance in preserving wavefront and/or in positioning optical elements and samples. Over the commissioning time of the first Sirius beamlines models and procedures have been continually improved. The next steps are related to more systematically analyzing the influences of temperature stability on the photon beam position.

ACKNOWLEDGEMENTS

The authors would like to gratefully acknowledge the funding by the Brazilian Ministry of Science, Technology and Innovation, and the contributions of the LNLS team.

REFERENCES

[1] Sirius project, https://www.lnls.cnpem.br/sirius-en/

[2] R. Geraldes *et al.*, "The New High Dynamics DCM for Sirius", in *Proc. MEDSI'16*, (Barcelona, Spain), Jun. 2017.

[3] M. S. Silva *et al.*, "Four-Bounce Crystal Monochromators for the Sirius/LNLS Beamlines", in *Proc. MEDSI'20*, (Chicago, USA), May 2021.

[4] R. Geraldes *et al.*, "The Design of Exactly-Constrained X-Ray Mirror Systems for Sirius", in *Proc. MEDSI'18*, (Paris, France), Dec. 2018.

[5] R. Geraldes *et al.*, "Design and Commissioning of the TARUMÃ Sta-tion at the CARNAÚBA Beamline at Sirius/LNLS", in *Proc. MEDSI'20*, (Chicago, USA), May 2021.

[6] R. Munnig Schmidt, G. Schitter, A. Rankers, and J. van Eijk, *The design of high performance mechatronics: high-tech functionality by multidisciplinary system integration (2nd revised edition)*, English. Netherlands: IOS Press, 2014, NEO, ISBN: 978-1-61499-367-4. DOI: 10.3233/978-1-61499-368-1-i.

[7] M. S. Silva, R. Geraldes, A. Gilmour, T. Ruijl, and R. Schneider, "Thermal Management and Crystal Clamping Concepts for the New High-Dynamics DCM for Sirius", in *Proc. MEDSI'16*, (Barcelona, Spain), Jun. 2017, pp. 194–197.

[8] F. Lena, R. Geraldes, M. S. Silva, and G. Moreno, "A Cryogenic Sample Environment for the TA-RUMÃ Station at the CARNAÚBA Beamline at Sirius/LNLS", in *Proc. MEDSI'20*, (Chicago, USA), May 2021.

[9] L. Arruda *et al.*, "Equipment and personal protection systems for the sirius beamlines", in *Proc. ICALEPCS'21*, (Shanghai, China), Oct. 2021.

ISBN: 978-3-95450-221-9 ISSN: 2226-0358 doi:10.18429/JACoW-ICALEPCS2021-WEPV001

[10] M. M. Donatti, D. H. C. Araujo, F. H. Cardoso, G. B. Z. L. Moreno, L. Sanfelici, and G. T. Semissatto, "Multi-channel heaters driver for sirius beamline optical devices", in *Proc. ICALEPCS'21*, (Shanghai, China), Oct. 2021.

[11] J. R. Piton, D. Alnajjar, D. H. C. Araujo, J. L. B. Neto, L. C. Guedes, and M. A. L. de Moraes, "Tatu: A flexible fpga-based trigger and timer unit created on compactrio for the first sirius beamlines", in *Proc. ICALEPCS'21*, (Shanghai, China), Oct. 2021.

[12] M. A. L. Moraes *et al.*, "The FPGA Control Implementation of the High-Dynamic Double-Crystal Monochromator at Sirius Light Source", in *ASPE 2020 Spring – Design and Control of Precision Mechatronic Systems*, (Boston, USA), ser. ASPE 2020 Spring – Design and Control of Precision Mechatronic Systems, May 2020, pp. 131–136.

[13] L. M. Volpe, J. C. Corsaletti, B. A. Francisco, R. R. Geraldes, and M. S. Silva, "Thermal model validation for the cryogenic mirror systems for sirius/lnls", in *Proc. MEDSI'20*, (Chicago, USA), JACoW Publishing, Jul. 2021.